## **ORGANOMETALLICS**

pubs.acs.org/Organometallics Article

# Allylic Amination of Pd(II)-Allyl Complexes via High-Valent Pd Intermediates

Yung-Ching Wang, Nigam P. Rath, and Liviu M. Mirica\*



Cite This: https://doi.org/10.1021/acs.organomet.2c00215



**ACCESS** I

III Metrics & More

Article Recommendations

s Supporting Information

**ABSTRACT:** Organometallic high-valent Pd(allyl) complexes have been recently proposed to act as intermediates in catalytic allylic functionalization reactions. While a few  $Pd^{IV}(\eta^1\text{-allyl})$  complexes have been isolated and characterized,  $Pd^{III}(\eta^3\text{-allyl})$  or  $Pd^{III}(\eta^1\text{-allyl})$  complexes have not been detected or isolated to date. Reported herein is the synthesis, characterization, and reactivity of a series of  $Pd^{II}(\eta^3\text{-allyl})$  complexes supported by the tetradentate pyridinophane ligands N,N'-di-tert-butyl-2,11-diaza-[3.3](2,6)pyridinophane ( $^{^{18}u}N4$ ) and N,N'-di-tert-methyl-2,11-diaza[3.3](2,6)pyridinophane ( $^{^{Me}N4}$ ). These  $Pd^{II}(\eta^3\text{-allyl})$  complexes exhibit accessible oxidation potentials and upon oxidation generate  $Pd^{III}(\text{allyl})$  complexes that were characterized by electron

paramagnetic resonance (EPR) spectroscopy. Interestingly, the  $[(^{Me}N4)Pd^{III}(\eta^3-allyl)]^{2+}$  complex undergoes a rearrangement to the  $[(^{Me}N4)Pd^{III}(\eta^1-allyl)]^{2+}$  species at low temperatures. Moreover, fast allylic amination occurred within 15 min at room temperature upon the reaction of  $[(^{Me}N4)Pd^{II}(\eta^3-allyl)]^+$  complexes with N-fluorobenzenesulfonimide (NFSI), and the C–N bond formation step is proposed to occur at the Pd(IV) oxidation state, likely via a  $Pd^{IV}(\eta^1-allyl)$  intermediate.

#### **■ INTRODUCTION**

 $Pd^{II}(\eta^3$ -allyl) complexes are key intermediates in Pd-catalyzed allylic functionalization reactions. <sup>1,2</sup> Since  $Pd^{II}(\eta^3$ -allyl) complexes were applied for the first time in carbon-carbon and carbon-heteroatom bond formation reactions by Tsuji et al.,3 the number of synthetic strategies and applications of  $Pd^{II}(\eta^3$ allyl) complexes has increased exponentially in the last decades.4 For example, the Tsuji-Trost reaction is one of the most common methods to form allylic products in organic synthesis. Furthermore, asymmetric allylic alkylation supported by chiral ligands has been widely explored in asymmetric total synthesis, and  $Pd^{II}(\eta^3$ -allyl) complexes proved to be essential intermediates in these transformations. In addition, high-valent Pd<sup>III</sup> and Pd<sup>IV</sup> complexes have been recognized as important intermediates in several oxidative transformations, 6-15 and earlier reports proposed the involvement of  $Pd^{IV}(\eta^3$ -allyl) complexes as intermediates in oxidative Pd-catalyzed allylic substitutions. <sup>16</sup> Although a few  $Pd^{IV}(\eta^1$ -allyl) complexes have been isolated or observed *in situ*, <sup>17–19</sup>  $Pd^{III}(\eta^1$ -allyl) or  $Pd^{IV}(\eta^3$ -allyl) complexes have yet to be isolated. Recently, our group has reported the characterization of Pd<sup>III</sup> and Pd<sup>IV</sup> complexes stabilized by the N,N'-di-alkyl-2,11-diaza[3.3](2,6)pyridinophane ( ${}^{R}N4$ , R =  ${}^{t}Bu$ ,  ${}^{i}Pr$ , Me) ligands and has studied their reactivity of C–C and C–heteroatom bond formation reactions. <sup>15,20–23</sup> Given the increasing significance of highvalent Pd complexes in chemical transformations, we proposed that the tetradentate RN4 ligands can also stabilize high-valent Pd<sup>III</sup>(allyl) or Pd<sup>IV</sup>(allyl) species. Reported herein are the

detection and characterization of a series of organometallic  $[(^RN4)Pd^{II}(allyl)]^{2+}$  complexes, as well as the allylic amination reactivity of  $[(^RN4)Pd^{II}(\eta^3-allyl)]^+$  complexes with N-fluorobenzenesulfonimide (NFSI).

#### ■ RESULTS AND DISCUSSION

The complex  $[(^{tBu}N4)Pd^{II}(\eta^3-allyl)]PF_6$   $(1^+\cdot PF_6)$  was synthesized by the reaction of  $^{tBu}N4$  with the  $[Pd^{II}(\eta^3-allyl)Cl]_2$  precursor and 2 equiv AgPF<sub>6</sub> in CH<sub>2</sub>Cl<sub>2</sub> (Scheme 1). X-ray characterization of a single crystal of  $1^+$  reveals a distorted square pyramid geometry around the  $Pd^{II}$  center, with one of the axial N atoms bound to the  $Pd^{II}$  center (Figure 1). Interestingly, the previously reported  $(^RN4)Pd^{II}$  complexes are commonly found in square planar geometries instead of square pyramidal geometries.  $^{15,20-23}$  The axial Pd1-N4 bond distance (2.612 Å) is longer than the average equatorial  $Pd1-N_{pyridyl}$  bond distance (2.133 Å). The average terminal Pd1-C bond distance (2.120 Å) and the C1-Pd1-C3 bond angle  $(68.5^\circ)$  are similar to those found in the previously reported  $[Pd^{II}(\eta^3-allyl)(di-2-pyridylsulfide)]^{+24}$  and  $[Pd^{II}(\eta^3-allyl)]$ 

Received: May 9, 2022



Scheme 1. Synthesis of ( $^{R}$ N4)Pd $^{II}$ ( $\eta^{3}$ -Allyl) Complexes 1 $^{+}$ -4 $^{+}$ 

allyl)(tetramethylethylenediamine)]+ complexes.<sup>25</sup> In our previous studies, different alkyl substituents (R = Me, 'Pr, <sup>t</sup>Bu) on the axial N atoms of <sup>R</sup>N4 ligands can tune the electronic properties and reactivity of (RN4)Pd complexes.<sup>26</sup> Therefore,  $^{Me}N4$  was also reacted with  $[Pd^{II}(\eta^3-allyl)Cl]_2$  and 2 equiv AgPF<sub>6</sub> to generate  $[(^{Me}N4)Pd^{II}(\eta^3-allyl)]PF_6(2^+\cdot PF_6)$ . X-ray characterization of a single crystal of 2+ also revealed a distorted square pyramidal geometry around the PdII center with one of the axial N atoms bound to the PdII center (Figure 1). Compared to the axial Pd1-N4 bond length (2.615 Å) of 1<sup>+</sup>, the axial Pd1-N2 bond distance (2.464 Å) of 2<sup>+</sup> is much shorter due to the less bulky N-methyl substituent in MeN4.<sup>27</sup> In contrast to the unequal equatorial Pd1-N<sub>pyridyl</sub> bond distances of 2.160 and 2.107 Å for 1+, the equatorial Pd1-N<sub>pyridyl</sub> bond distances of 2.137 Å for 2<sup>+</sup> are equal, which suggests  $2^+$  is more symmetrical than  $1^+$ . The [Pd<sup>II</sup>( $\eta^3$ cinnamyl)Cl]<sub>2</sub> and [Pd<sup>II</sup>( $\eta^3$ -2-methylallyl)Cl]<sub>2</sub> precursors were also reacted with the tBuN4 ligand to potentially synthesize the corresponding  $[(^{tBu}N4)Pd^{II}(\eta^3\text{-cinnamyl})]^+$  and  $[(^{tBu}N4)\text{-}$  $Pd^{II}(\eta^3-2-methylallyl)]^+$  complexes; however, the formation of the corresponding ( $^{fBu}N4$ ) $Pd^{II}$  complexes was hindered by the steric clash between the bulky N-<sup>t</sup>Bu groups of the <sup>tBu</sup>N4 ligand and the  $\eta^3$ -cinnamyl or  $\eta^3$ -2-methylallyl groups. In contrast, the less bulky MeN4 ligand was successfully used to synthesize  $[(^{Me}N4)Pd^{II}(\eta^3\text{-cinnamyl})]PF_6$  (3+•PF<sub>6</sub>) in 82% yield. X-ray characterization of a single crystal of 3<sup>+</sup> reveals a distorted square pyramid geometry around the Pd<sup>II</sup> center with

a syn orientation of the  $\eta^3$ -cinnamyl moiety (Figure 1). For  $3^+$ , the Pd1–C1 bond distance of 2.088 Å is slightly shorter than the Pd1–C2 bond distance of 2.111 Å, while the Pd1–N1 bond distance (2.164 Å) is slightly longer than the Pd1–N2 bond distance of 2.131 Å. As a result, the longer Pd1–N1 bond is trans to the shorter Pd1–C1 bond, which is contrary to the relative Pd–N and Pd–C bond lengths in the [(tmeda)-Pd<sup>II</sup>( $\eta^3$ -cinnamyl)]<sup>+</sup> complex.<sup>28</sup> The [(MeN4)Pd<sup>II</sup>( $\eta^3$ -2-methylallyl)]PF<sub>6</sub> (4+PF<sub>6</sub>) complex was also successfully synthesized and isolated in 85% yield. X-ray characterization of a single crystal of 4<sup>+</sup> also reveals a distorted square pyramidal geometry at the Pd<sup>II</sup> center (Figure 1), with the methyl group of  $\eta^3$ -allyl moiety pointing down due to the steric hindrance generated by the axial N-methyl groups of the MeN4 ligand.

Interestingly, the methylene groups on <sup>fBu</sup>N4 of 1<sup>+</sup> show two broad peaks in the <sup>1</sup>H NMR spectrum at RT, suggesting a rapid exchange between the two axial N donors with one binding to the Pd center (Figure 2, top), as well as a rapid rotation of the allyl group, given the well-established fluxionality of the Pd-allyl complexes.<sup>29,30</sup> Moreover, variable temperature NMR experiments reveal that lowering the temperature to -50 °C leads to the appearance of four welldefined doublet peaks in the <sup>1</sup>H NMR spectrum for 1<sup>+</sup> at 3.93, 4.50, 4.72, and 4.94 ppm, which indicate that one of the axial N-methyl donors is locked onto the PdII center at low temperature and as observed previously for related cationic Pd<sup>II</sup> complexes.<sup>31</sup> By comparison, the methylene groups of 2<sup>+</sup> show two doublet peaks in the <sup>1</sup>H NMR spectrum at RT (Figure S3), which suggests that the two axial N atoms are likely not bound to the Pd<sup>II</sup> center in solution, given the preferred square planar geometry of Pd<sup>II</sup> centers. <sup>15,20–23,31</sup> The methylene groups of 4<sup>+</sup> also show two doublet peaks, which is consistent with the methylene groups of 2<sup>+</sup> in the <sup>1</sup>H NMR spectrum at RT (Figure S7). By contrast, the methylene groups of 3+ show one broad peak and two doublet peaks in the <sup>1</sup>H NMR spectrum at RT (Figure S5), suggesting a rapid exchange between two axial N donors is not favorable. Therefore, the structure of 3<sup>+</sup> prefers to be a five-coordinate square pyramidal geometry in solution, which is in line with its solid-state structure. The  $^{1}H$  NMR spectrum of  $\eta^{3}$ -cinnamyl moiety in  $3^+$  shows two trans ( ${}^3J = 10.8 \text{ Hz}$ ) coupling and only one cis coupling ( ${}^{3}I = 6.4 \text{ Hz}$ ), suggesting the phenyl group is a

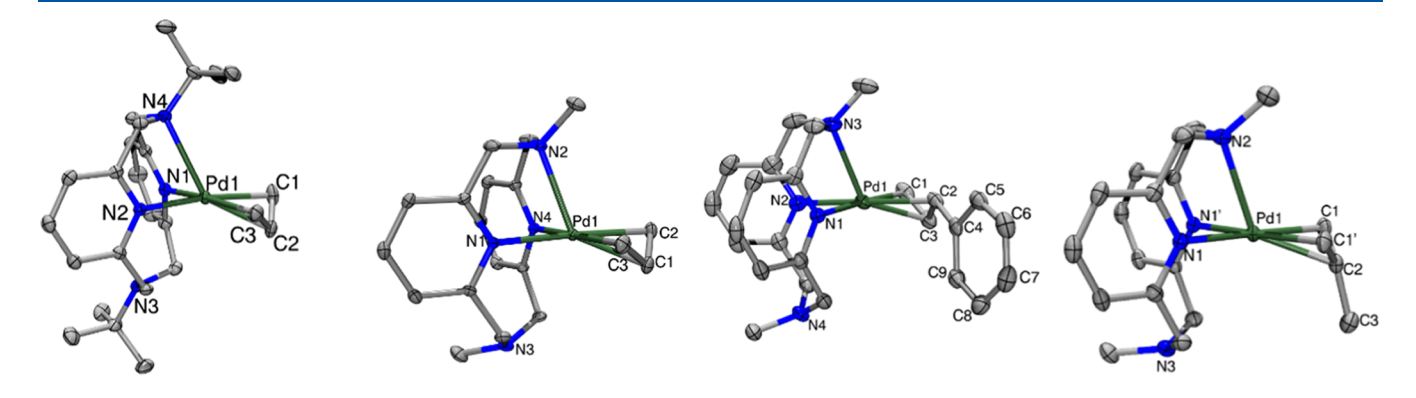


**Figure 1.** ORTEP representation (50% probability ellipsoids) of anions 1<sup>+</sup>, 2<sup>+</sup>, 3<sup>+</sup>, and 4<sup>+</sup> (from left to right). Selected bond distances: 1<sup>+</sup>, Pd1-N1 2.160(14), Pd1-N2 2.107 (14), Pd1-N4 2.615(1), Pd1-C1 2.117 (18), Pd1-C2 2.104 (17), and Pd1-C3 2.122 (16); 2<sup>+</sup>, Pd1-N1 2.137 (5), Pd1-N2 2.464 (8), Pd1-N4 2.137 (5), Pd1-C1 2.116(9), Pd1-C2 2.108(7), and Pd1-C3 2.108(7); 3<sup>+</sup>, Pd1-N1 2.164 (2), Pd1-N2 2.131(2), Pd1-N3 2.434(2), Pd1-C1 2.088(3), Pd1-C2 2.111(3), and Pd1-C3 2.135(3); 4<sup>+</sup>, Pd1-N1 2.134(2); Pd1-N1 2.134(2), Pd1-N2 2.475(2), Pd1-C1 2.103(3), Pd1-C1 2.103(3), and Pd1-C2 2.147(3).

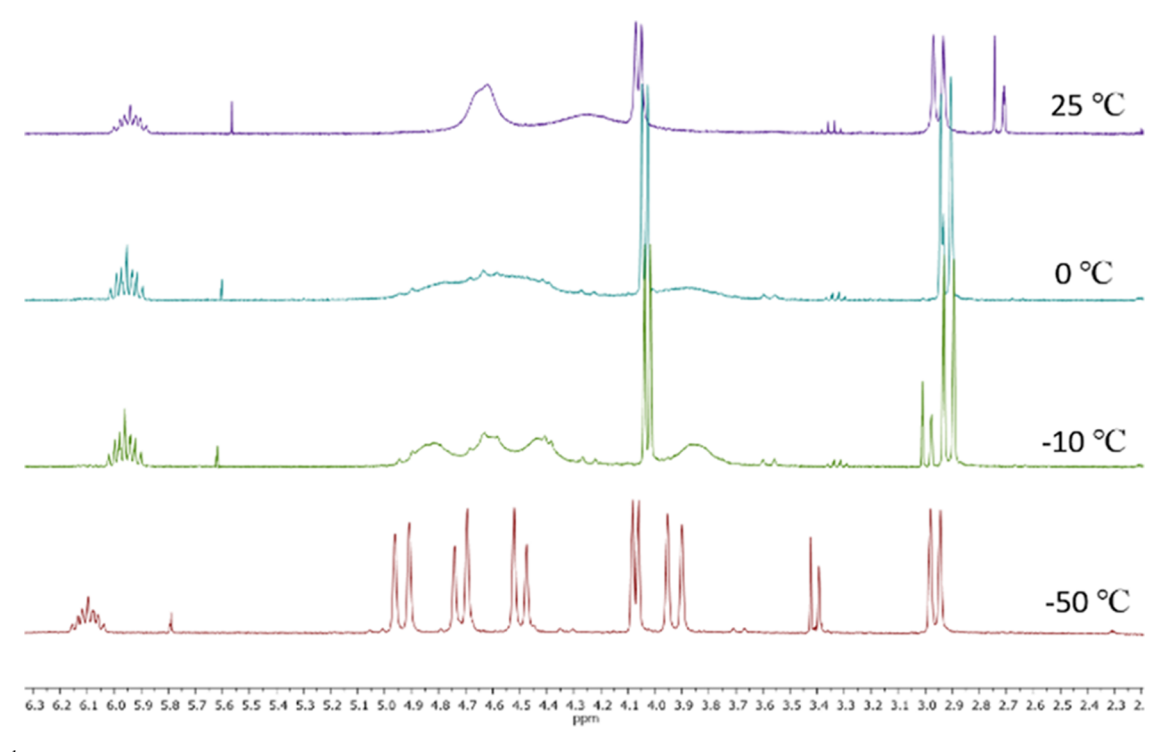


Figure 2. <sup>1</sup>H NMR variable temperature experiment of 1<sup>+</sup> in acetone- $d_6$ . The peaks at ~2.7 ppm in the RT correspond to H<sub>2</sub>O and HOD, respectively, and they shift to ~3.4 ppm at -50 °C. <sup>32</sup>

*syn* position in solution, which matches the solid-state structure of  $3^+$ . Thus, we can conclude that the *syn*—anti isomerization is absent in solution at RT.

The cyclic voltammetry (CV) of 1<sup>+</sup> in 0.1 M tetrabutylammonium hexafluorophosphate (Bu<sub>4</sub>NPF<sub>6</sub>)/acetonitrile (MeCN) exhibits an irreversible oxidation wave at 942 mV vs ferrocene/ferrocenium (Fc+/Fc), which is tentatively assigned to the Pd<sup>II/III</sup> redox couple (Figure 3 and Table 1). The CV of 2<sup>+</sup> in 0.1 M Bu<sub>4</sub>NPF<sub>6</sub>/MeCN reveals three reversible waves at 93, 595, and 885 mV vs Fc<sup>+</sup>/Fc. Similarly, the CVs of  $3^+$  and  $4^+$  exhibit three reversible waves at 79, 515, and 755 mV vs  $Fc^+/Fc$  for  $3^+$ , and 210, 590, and 950 mV vs Fc<sup>+</sup>/Fc for 4<sup>+</sup>, respectively. Since the <sup>Me</sup>N4 ligand is not redoxactive within this potential range, the first and second reversible waves are both tentatively assigned to the PdII/III redox couple, since the MeN4 ligand can adopt either a  $\kappa^4$  or  $\kappa^3$ binding mode.<sup>31</sup> Comparing the CV of 1<sup>+</sup> with that of 2<sup>+</sup>, a higher oxidation potential with an increase in ligand steric bulk from MeN4 to tBuN4 is observed, as seen previously for the  $(^{\text{Me}}\text{N4})\text{Pd}^{\text{II}}(\text{CH}_3)_2$  vs  $(^{^{\text{IBu}}}\text{N4})\text{Pd}^{\text{II}}(\text{CH}_3)_2$  or the  $(^{\text{Me}}\text{N4})$ -Pd $^{\text{II}}(\text{CH}_3)\text{Cl}$  vs  $(^{^{\text{IBu}}}\text{N4})\text{Pd}^{\text{II}}(\text{CH}_3)\text{Cl}$  complexes. $^{^{22}}$ 

The low  $Pd^{II/III}$  redox potentials allowed for the use of chemical oxidants to generate the corresponding  $Pd^{III}$  intermediates, which were characterized by electron paramagnetic resonance (EPR) spectroscopy. The EPR spectrum of the species formed upon the oxidation of  $1^+$  with thianthrenyl hexafluorophate ( $[Thn^{\bullet+}]PF_6$ ) at -40 °C reveals a rhombic signal with the  $g_{ave}$  value of 2.112 corresponding to the  $Pd^{III}$  d<sup>7</sup> metal center in the  $d_z^2$  ground state (Figure 4). The quintet superhyperfine coupling in the  $g_z$  region ( $A_z(2N) = 22.0$  G) is attributed to the interaction with the two axial N atoms (I = 1), suggesting that the distorted octahedral geometry of  $1^{2+}$  is maintained in solution (Scheme 2), while a rapid rotation of the allyl group is expected to still be operative, given the well-established fluxionality of the Pd-allyl

complexes.<sup>29,30</sup> Unfortunately, the complex 1<sup>2+</sup> was highly unstable and decayed within 1 min to generate an EPR-silent species. Because of the lower Pd<sup>II/III</sup> redox potentials of the (MeN4)Pd<sup>II</sup> complexes, acetylferrocenium hexafluorophosphate (AcFcPF<sub>6</sub>) was used to generate the corresponding Pd<sup>III</sup> species. For the oxidation of 2<sup>+</sup>, while the oxidation potential of Pd<sup>II/III</sup> was accessible by AcFcPF<sub>6</sub>, no EPR signal was observed at -35 °C. Subsequently, we presumed the corresponding Pd<sup>III</sup> complex was unstable at -35 °C.

To obtain the Pd<sup>III</sup> species 2<sup>2+</sup>, [Thn<sup>•+</sup>]PF<sub>6</sub> was added to the MeCN solution of 2<sup>+</sup> at −94 °C. Intriguingly, the EPR spectrum of 22+ shows two different EPR signals, suggesting there are two corresponding Pd<sup>III</sup> complexes present upon oxidation (Figure 5a) and tentatively assigned as the  $[(^{\text{Me}}\text{N4})\text{Pd}^{\text{III}}(\eta^3\text{-allyl})]^{2+}$   $(\eta^3\text{-}2^{2+})$  species and the  $[(^{\text{Me}}\text{N4})\text{-}$  $Pd^{III}(\eta^1$ -allyl)]<sup>2+</sup> ( $\eta^1$ -2<sup>2+</sup>) species, respectively (Schemes 2 and 3). The two EPR species decayed while warming up from -94°C to RT. The EPR spectrum of  $\eta^3$ -2<sup>2+</sup> at -94 °C reveals a quasi-rhombic signal with the gave value of 2.090 corresponding to the Pd<sup>III</sup> d<sup>7</sup> metal center (Figure 5b). The superhyperfine coupling of  $\eta^3$ -2<sup>2+</sup> reveals there are two axial N atom donors  $(A_z(2N) = 24.0 \text{ G})$  binding to the Pd<sup>III</sup> center. The EPR spectrum of  $\eta^1$ -2<sup>2+</sup> formed upon 5 min warmup at -40 °C displays a rhombic signal with the  $g_{ave}$  value of 2.152 corresponding to the Pd<sup>III</sup> d<sup>7</sup> metal center, along with the superhyperfine coupling from the two axial N atoms  $(A_z(2N))$ = 20.0 G, Figure 5c). Notably, the superhyperfine coupling constant in  $\eta^{1}$ -2<sup>2+</sup> is smaller, suggesting the Pd<sup>III</sup> species in  $\eta^{1}$ -22+ has a weaker binding interaction between the two axial N arms and the Pd<sup>III</sup> center. This effect could be a result of a strong  $\sigma$ -donating ligand at the Pd<sup>III</sup> center. Therefore, we propose the Pd<sup>III</sup> species in  $\eta^3$ -2<sup>2+</sup> is the [(MeN4)Pd<sup>III</sup>( $\eta^3$ -allyl)]<sup>2+</sup> complex and the Pd<sup>III</sup> species in  $\eta^1$ -2<sup>2+</sup> is the  $[(M^{e}N4)Pd^{III}(\eta^{1}-allyl)]^{2+}$  complex, since  $\eta^{1}$ -allyl ligand has stronger  $\sigma$ -donating ability than a  $\eta^3$ -allyl ligand (Scheme 2).

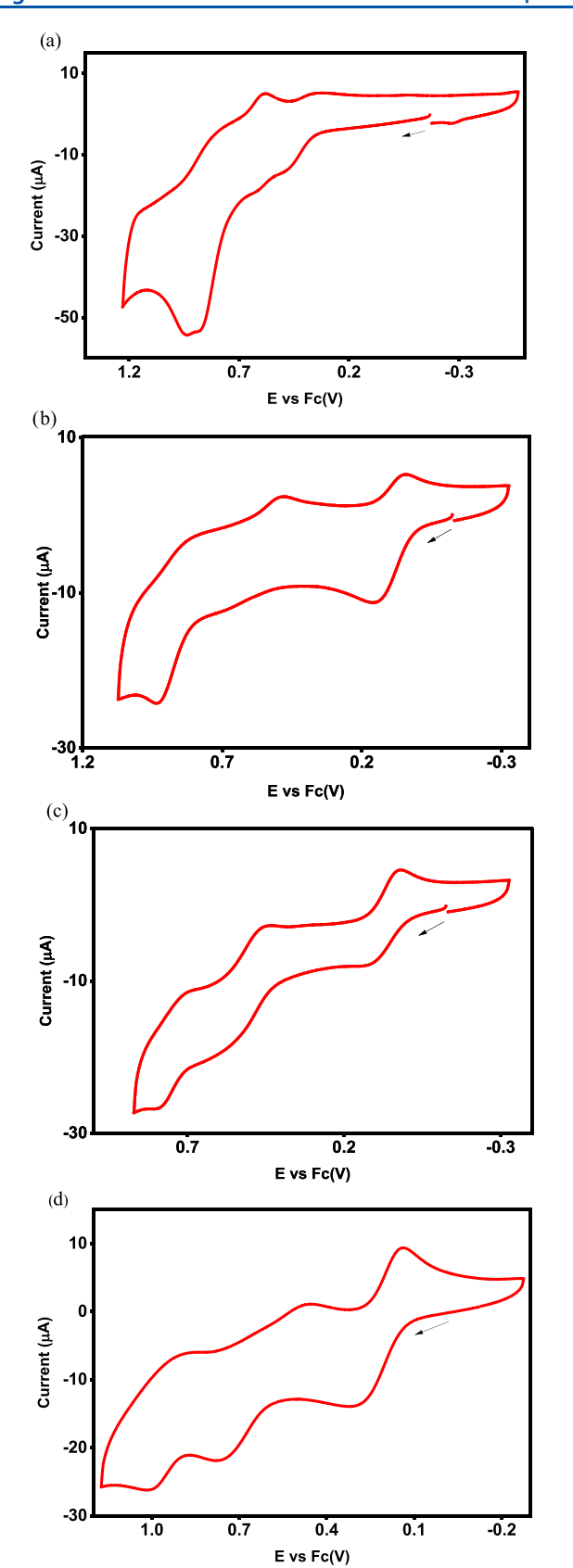
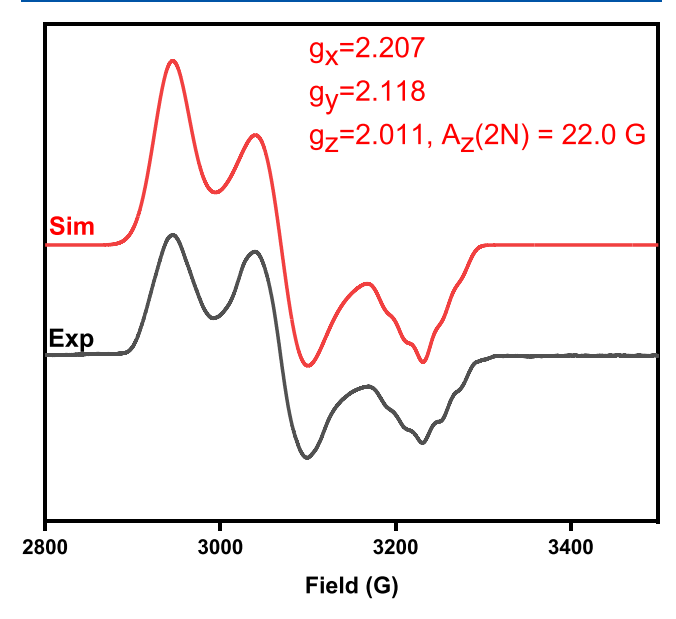


Figure 3. CV of  $1^+$  (a),  $2^+$  (b),  $3^+$  (c), and  $4^+$  (d) in 0.1 M Bu<sub>4</sub>NPF<sub>6</sub>/MeCN (scan rate =100 mV/s).

Moreover, the geometry of  $\eta^3$ -2<sup>2+</sup> is more symmetrical than that of  $\eta^1$ -2<sup>2+</sup>, which may cause a pseudo-axial EPR signal in  $\eta^3$ -2<sup>2+</sup>, comparable to a rhombic EPR signal in  $\eta^1$ -2<sup>2+</sup>. With the

Table 1. Redox Potentials of Complexes 1<sup>+</sup>-4<sup>+</sup>

complex	$E_{\mathrm{pa}}(\mathrm{Pd^{II/III}}) \ \mathrm{(mV)}$	$E_{\rm pc}({ m Pd}^{ m III/II}) \ ({ m mV})$	$E_{\mathrm{pa}}(\mathrm{Pd^{III/IV}}) \ \mathrm{(mV)}$	$E_{\rm pc}({ m Pd}^{ m IV/III}) \ ({ m mV})$
1+	942	840		
2+	150, 700	36, 490	930	840
<b>3</b> <sup>+</sup>	140, 570	17, 460	800	710
4+	290, 720	130, 460	1000	900



**Figure 4.** Experimental (1:3 MeCN/PrCN glass, 77 K) and simulated EPR spectra of  $\mathbf{1}^{2+}$ . The following parameters were used for simulations:  $\mathbf{1}^{2+}$ ,  $g_x = 2.207$ ;  $g_y = 2.118$ ;  $g_z = 2.011$  ( $A_z(2N) = 22.0$  G).

EPR simulations of  $\eta^3$ -2<sup>2</sup> and  $\eta^1$ -2<sup>2+</sup>, the EPR spectrum of the oxidation of  $2^+$  in 30 s at -94 °C has a 1.3:1 ratio of  $\eta^3$ - $2^{2+}$  to  $\eta^{1}$ -2<sup>2+</sup> (Figure S14d). After a 10-min warmup at -94 °C, the ratio of  $\eta^{3}$ -2<sup>2+</sup> to  $\eta^{1}$ -2<sup>2+</sup> is 1:2.2 (Figure S14e). Further warmups at RT caused immediate decay of both  $\eta^3$ -2<sup>2+</sup> and  $\eta^1$ - $2^{2+}$ . Based on these EPR results, we assume  $\eta^3$ - $2^{2+}$  was formed first from the oxidation of  $2^+$  (Figure 5a). Then,  $\eta^3$ - $2^{2+}$  decayed within minutes at -94 °C (black arrow, Figure 5a) and converted to  $\eta^{1}$ -2<sup>2+</sup>, which formed predominantly after 10 min at -94 °C (red arrow). Subsequently, both  $\eta^3$ -2<sup>2+</sup> and  $\eta^3$ -2<sup>2+</sup> decomposed rapidly upon warming up to RT. Notably, the allyl ligand in high-valent Pd<sup>IV</sup> complexes prefers to adopt a  $\eta^1$ bonding mode, as observed for the two reported high-valent  ${\rm Pd^{IV}}$  complexes with a  $\eta^1$ -allyl ligand. However, these two high-valent  $Pd^{IV}(\eta^1$ -allyl) complexes were unstable and were only detected by the low-temperature <sup>1</sup>H NMR. To the best of our knowledge, this is the first observation of the conversion of high-valent  $[(M^eN4)Pd^{III}(\eta^3-allyl)]^{2+}$  to  $[(M^eN4)Pd^{III}(\eta^1-allyl)]$ <sup>2+</sup> intermediates (Scheme 3).

The oxidation of  $3^+$  at -78 °C exhibits a complicated EPR signal (Figure 6), and the EPR simulation suggests more than one more Pd<sup>III</sup> species exist upon oxidation of  $3^+$ ; the possibility that the phenyl group interacts directly with the Pd center cannot be excluded. The best EPR simulation of  $3^{2+}$  reveals a rhombic signal with the  $g_{\rm ave}$  value of 2.109 and the superhyperfine coupling from the two axial N donors ( $_{Ax}(2N) = 25.0 \; {\rm G}; A_y(2N) = 80.0 \; {\rm G}; A_z(2N) = 19.0 \; {\rm G}$ ) observed in the  $g_{xy}$ ,  $g_{yy}$ , and  $g_z$  regions. However, the corresponding Pd<sup>III</sup> complexes decay within 1 min at RT. The EPR spectrum of the oxidation of  $4^+$  at -78 °C reveals an isotropic signal with

Scheme 2. Oxidation of Pd<sup>II</sup> Complexes 1<sup>+</sup>-4<sup>+</sup> to Generate Pd<sup>III</sup>-Allyl Species

the  $g_{\text{ave}}$  value of 2.102, along with the superhyperfine coupling from the two axial N atoms  $(A_{z}(2N) = 24.0 \text{ G})$  observed in the  $g_z$  region, suggesting an octahedral geometry at the Pd<sup>III</sup> d<sup>7</sup> metal center in the d<sub>z</sub><sup>2</sup> ground state (Figure 6). The superhyperfine coupling  $(A_z(2N) = 24.0 \text{ G})$  in  $4^{2+}$  suggests the presence of the  $\eta^3$ -2-methylallyl ligand at the Pd<sup>III</sup> center, which is consistent with the superhyperfine coupling  $(A_z(2N))$ = 24.0 G) in  $\eta^3$ -2<sup>2+</sup>. Furthermore, we did not observe an EPR signal corresponding to  $[(^{\text{Me}}\text{N4})\text{Pd}^{\text{III}}(\eta^{\text{1-2-methylallyl}})](\text{PF}_6)_2$  when  $[\text{Thn}^{\bullet+}]\text{PF}_6$  was added into the MeCN solution of 4<sup>+</sup> at −94 °C. Consequently, [(MeN4)Pd<sup>III</sup>(2-methylallyl)]<sup>2+</sup> would prefer to be in the  $\eta^3$ -allyl coordination mode due to the additional methyl group at the C2 position of the allyl ligand. Indeed, the EPR spectrum of 42+ reveals an isotropic signal, suggesting the structure of the corresponding Pd<sup>III</sup> is more symmetric and likely due to a  $\eta^3$ -allyl coordination mode of the  $\eta^3$ -2-methylallyl ligand. While the EPR signal of  $4^{2+}$  remains unchanged for 15 min at RT, suggesting a fairly stable PdIII complex, several attempts to isolate and structurally characterize 4<sup>2+</sup> in different solvent combinations were unsuccessful. Although we were unable to get an X-ray quality crystal of  $4^{2+}$ , to the best of our knowledge, this is the first stable high-valent  $[Pd^{III}(\eta^3-2-methylallyl)]^{2+}$  complex adopting a  $\eta^3$ -allyl bonding mode.

To support the proposed structures for the Pd<sup>III</sup> species, density functional theory (DFT) calculations were performed, and the resulting metrical parameters for the optimized geometries of  $[(^{Me}N4)Pd^{III}(\eta^3-allyl)]^{2+}$  complexes  $\eta^1-2^{2+}$ ,  $\eta^3-2^{2+}$  $2^{2+}$ ,  $3^{2+}$ , and  $4^{2+}$  were investigated and compared to the previously characterized [(MeN4)PdIIIMeCl]+ (6+, Figure 7). For  $\eta^3 - 2^{2+}$  and  $4^{2+}$ , the electron densities of their corresponding LUMOs are localized mainly along the axial direction, with contributions from the axial N atoms of 24% for  $\eta^3$ -2<sup>2+</sup> and 23% for 4<sup>2+</sup>, respectively. In contrast, the lower 22% contribution from the axial N atoms of  $6^+$  is in line with the stronger  $\sigma$ -donating ligand (methyl vs  $\eta^3$ -allyl) that decreases the binding interaction from the axial N atoms to the PdIII center. For 3<sup>2+</sup>, the lower 22% contribution from the axial N atoms is also likely caused by the steric hindrance from the phenyl group of the cinnamyl ligand that weakens the axial binding interaction. Accordingly, the minimized structure of  $\eta^{1}$ -2<sup>2+</sup> has a 22% contribution from the axial N atoms, suggesting the  $\eta^1$ -allyl ligand is a stronger  $\sigma$ -donating group, which is identical to 22% contribution from the axial N atoms of 6<sup>+</sup>, which contains methyl ligands. The 4% contribution from the  $\eta^3$ -allyl ligand of  $\eta^3$ -2<sup>2+</sup> and 4<sup>2+</sup> also indicates that the  $\eta^3$ -allyl ligand is a weak  $\sigma$ -donating group, comparable to the

7% contribution from the  $\eta^1$ -allyl ligand of  $\eta^1$ - $2^{2+}$ . Consequently, the less  $\sigma$ -donating ligands ( $\eta^1$ -allyl ligand vs  $\eta^3$ -allyl ligand) result in a weaker binding interaction between the Pd<sup>III</sup> center and the axial N atoms, which is in line with the weaker superhyperfine couplings in the  $g_z$  direction ( $A_z(2N) = 24.0$  G for  $\eta^3$ - $2^{2+}$ ,  $A_z(2N) = 24.0$  G for  $4^{2+}$ , and  $A_z(2N) = 20.0$  G for  $\eta^1$ - $2^{2+}$ ). The calculated superhyperfine coupling ( $A_z(2N) = 22.2$  G) for  $\eta^1$ - $2^{2+}$  is smaller than the calculated superhyperfine coupling ( $A_z(2N) = 24.2$  G) for  $\eta^3$ - $2^2$ , providing further support that the  $\eta^1$ -allyl ligand is a stronger  $\sigma$ -donating ligand vs to the  $\eta^3$ -allyl ligand and the structural assignments for the observed EPR species. Finally, the calculated superhyperfine coupling ( $A_z(2N) = 24.2$  G) matches the experimental superhyperfine coupling ( $A_z(2N) = 24.2$  G) for  $\eta^3$ - $2^{2+}$  (Table 2).

The calculated superhyperfine couplings are similar to the experimental superhyperfine couplings for  $\eta^3$ -2<sup>2+</sup>,  $\eta^1$ -2<sup>2+</sup>, 3<sup>2+</sup>, and 4<sup>2+</sup> (Table 2). The calculated superhyperfine coupling constant of  $A_{r}(2N) = 19.1$  G for  $\mathbf{1}^{2+}$  is smaller than the calculated superhyperfine coupling constant  $A_z(2N) = 24.2$  G for  $\eta^3$ -2<sup>2+</sup>, which is attributable to the bulky N-<sup>t</sup>Bu groups weakening the axial interaction. The experimental superhyperfine coupling constant of  $A_z(2N) = 22.0$  G measured for  $1^{2+}$  also implies that the allyl ligand adopts a  $\eta^3$  coordination mode. Otherwise, if  $1^{2+}$  adopts a the  $\eta^{1}$ -allyl coordination, an experimental superhyperfine coupling constant smaller than 20.0 G would be expected, comparable to the value of  $A_z(2N)$  = 20.0 G observed for  $\eta^1$ -2<sup>2+</sup> (Figure 5b). Finally, the calculated superhyperfine coupling constant of  $A_z(2N) = 20.7$ G for  $3^{2+}$  is close to the experimental value of  $A_z(2N) = 19.0$ G, suggesting the cinnamyl ligand binds to the Pd<sup>III</sup> center in a  $\eta^3$  binding mode.

 ${
m Pd^{II}}({
m allyl})$  complexes have been previously established as intermediates toward forming allylic substitution products such as allylamine and allyl acetate.  ${
m ^{33-37}}$  The reaction conditions usually require higher temperatures or longer reaction times for the  ${
m Pd^{0/II}}$ -catalyzed allylic substitution reactions.  ${
m ^{38,39}}$  Recent reports reveal three chemical oxidants (PhI(OAc)2, PhICl2, and NFTPT) that have been used to oxidize the  ${
m Pd^{II}}$  complexes to the stable  ${
m Pd^{IV}}$  complexes containing a OAc, Cl, or F ligand.  ${
m ^{40-43}}$  These  ${
m Pd^{IV}}$  complexes can undergo fast reductive elimination to make C–Cl, C–F or C–OAc bond formation products. Since our  $[({
m ^{Me}N4}){
m Pd^{II}}(\eta^3$ -allyl)]+ complexes proved to be easily oxidized to high-valent Pd species, we performed preliminary investigations of the reactivity of  ${
m 2^+}$ ,  ${
m 3^+}$ , and  ${
m 4^+}$  toward C–Cl and C–OAc bond formations using PhICl2 and PhI(OAc)2.  ${
m ^{44,45}}$  However, we did not observe  ${
m Pd^{IV}}$ 

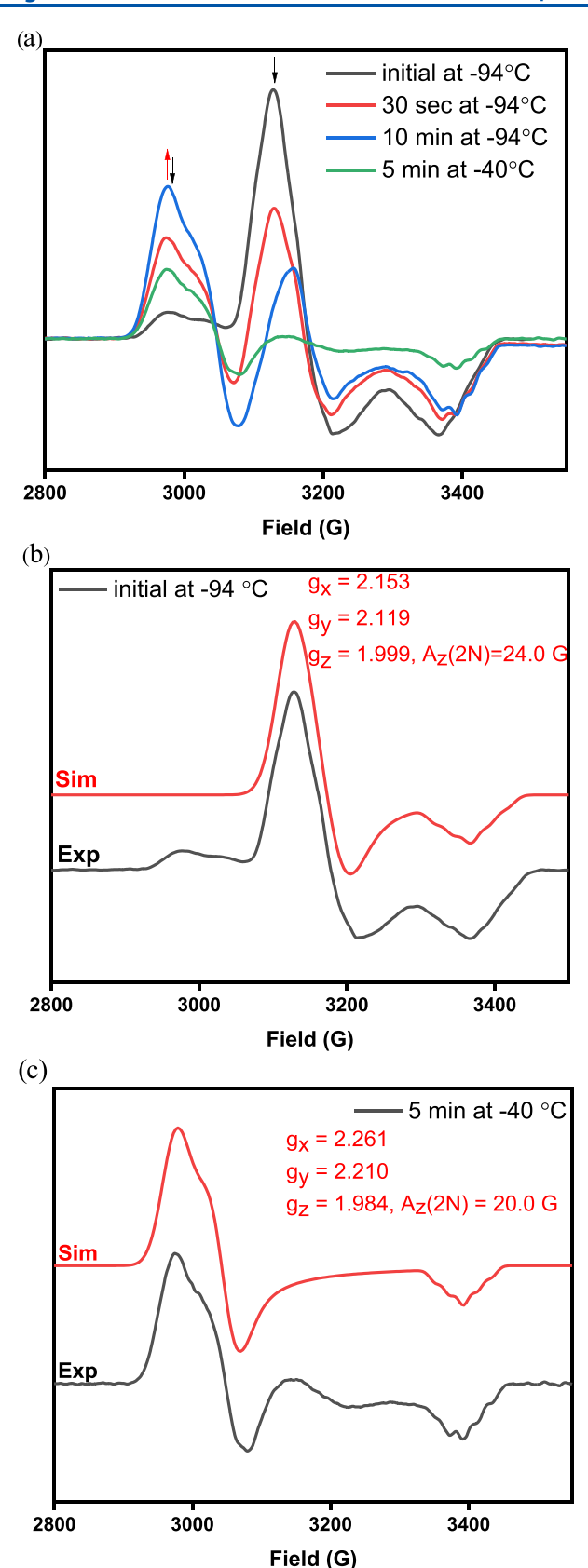
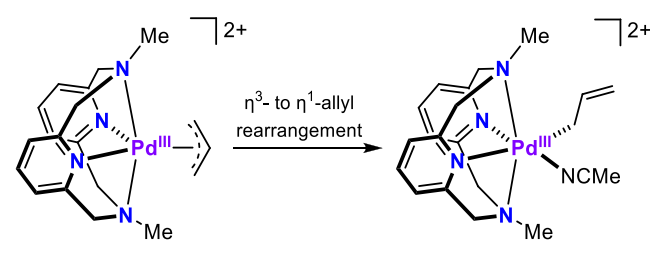


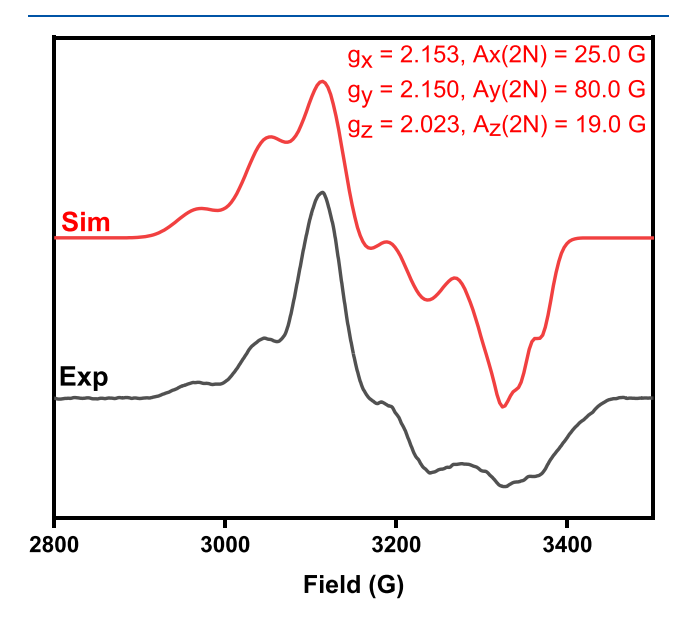
**Figure 5.** EPR spectrum of  $η^3$ -2<sup>2+</sup> and  $η^1$ -2<sup>2+</sup> in 3:1 PrCN/MeCN glass, 77 K. (a) Variable time and temperature EPR spectrum of the oxidation of 2<sup>+</sup>. (b) Simulation  $η^3$ -2<sup>2+</sup>,  $g_x$  = 2.153;  $g_y$  = 2.119;  $g_z$  = 1.999 ( $A_z$ (2N) = 24.0 G). (c) Simulation  $η^1$ -2<sup>2+</sup>,  $g_x$  = 2.261;  $g_y$  = 2.210;  $g_z$  = 1.984 ( $A_z$ (2N) = 20.0 G).

Scheme 3. Proposed Rearrangement from the  $\eta^3$ -2<sup>2+</sup> to the  $\eta^1$ -2<sup>2+</sup> Species



 $[(^{Me}N4)Pd^{III}(\eta^3\text{-allyl})]^{2+}(\eta^3\text{-}2^{2+})$ 

 $[(^{Me}N4)Pd^{III}(\eta^{1}\text{-allyl})]^{2+}(\eta^{1}\text{-}2^{2+})$ 



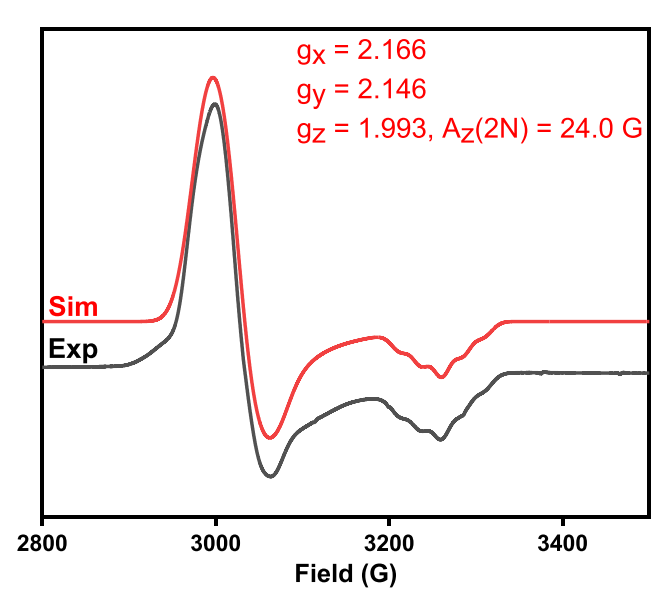


**Figure 6.** Experimental (1:3 MeCN/PrCN glass, 77 K) and simulated EPR spectra of  $3^{2+}$  (top),  $4^{2+}$  (bottom). The following parameters were used for simulations:  $3^{2+}$ ,  $g_x = 2.153$  ( $_{Ax}(2N) = 2.06$  G);  $g_y = 2.146$  ( $A_y(2N) = 80.0$  G);  $g_z = 2.023$  ( $A_z(2N) = 19.0$  G);  $4^{2+}$ ,  $g_x = 2.166$ ;  $g_y = 2.146$ ; and  $g_z = 1.993$  ( $A_z(2N) = 24.0$  G).

complexes bearing OAc or Cl ligands, nor C–Cl or C–OAc bond formation products from the reaction of  $2^+-4^+$  with PhICl<sub>2</sub> and PhI(OAc)<sub>2</sub> (Table S2). The trifluoromethyl

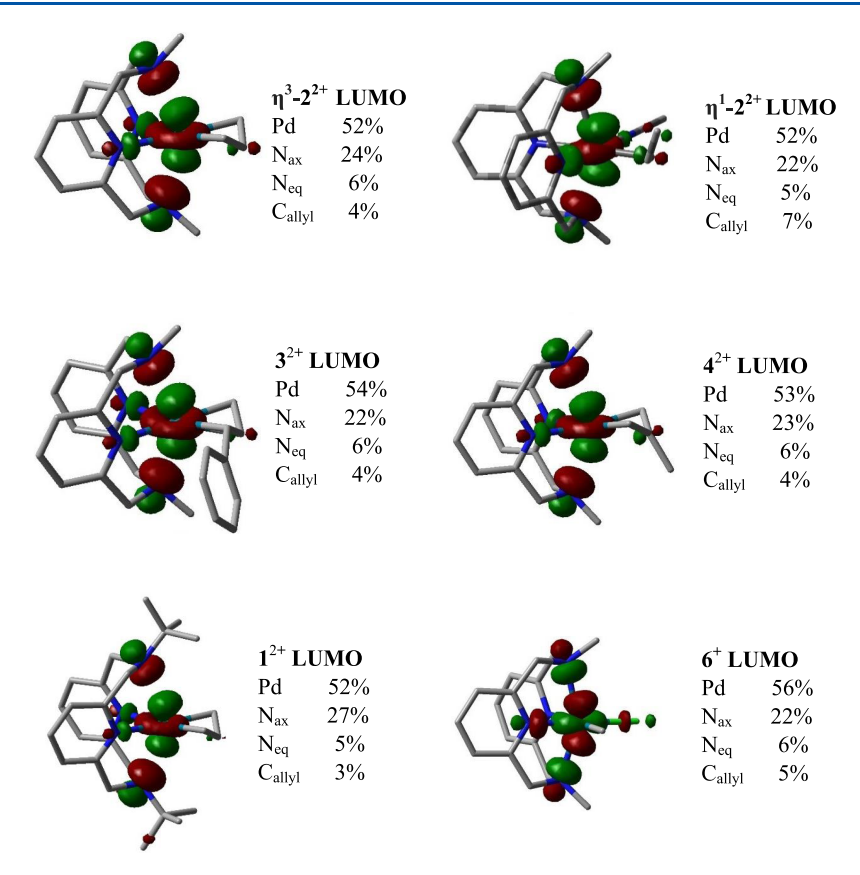


Figure 7. DFT-calculated (UB3LYP/Def2-TZVP) molecular orbitals ( $\beta$  LUMOs) of  $\eta^3$ -2<sup>2+</sup> (top left),  $\eta^1$ -2<sup>2+</sup> (top right) 3<sup>2+</sup> (middle left), 4<sup>2+</sup> (middle right), the MeN4-supported complexes 6<sup>+</sup> (bottom right) and 1<sup>2+</sup> (bottom left), and the calculated atomic contributions.

Table 2. Comparison of Experimental and DFT-Calculated N Superhyperfine Coupling Constants for  $Pd^{\rm III}$  Complexes  $1^{2+}-4^{2+}$ 

	$A_z(2N)$	), G
complex	experimental	calculated
1 <sup>2+</sup>	22.0	19.1
$\eta^{3}$ -2 <sup>2+</sup> $\eta^{1}$ -2 <sup>2+</sup> $3^{2+}$	24.0	24.2
$\eta^{\scriptscriptstyle 1}$ -2 $^{\scriptscriptstyle 2^+}$	20.0	22.2
	19.0	20.7
4 <sup>2+</sup>	24.0	21.6

reagents are reported to isolate stable PdIV-CF3 complexes, which is followed by the reductive elimination to form C-CF<sub>3</sub> bond products.46 Thus, we examined the C-CF3 bond formation reactivity upon the reaction of  $2^+-4^+$  with 1trifluoromethyl-1,2-benziodoxol-3-(1H)-one (I-CF<sub>3</sub>) and 5-(trifluoromethyl)dibanzothiophenium (S-CF<sub>3</sub>). Unfortunately, none of these reactions produced the desirable C-CF<sub>3</sub> products. We then probed the C-F bond formation reactivity using 1-fluoro-2,4,6-trimethylpyridinium triflate (NFTPT) and N-fluorobenzenesulfonimide (NFSI) as F+ reagents.<sup>47-</sup> Interestingly, the color of the reaction of  $2^+-4^+$  with 2 equiv NFSI in MeCN changed from yellow to purple at room temperature, and the terminal amine products were formed in 48-58% yield within 15 min (Table 3). Interestingly, when NFSI was added to the solutions of  $2^+-4^+$  at -35 °C, the yields of amination products increased to 70-78%. By comparison, no color change was observed for the reaction of 1<sup>+</sup> with 2 equiv NFSI in MeCN, and the amination product was formed in only 21% yield after 24 h, suggesting that NFSI

Table 3. Yields of the Amination Products Upon the Reaction of  $1^+-4^+$  with NFSI

$$(^{R}N4)^{Pd}$$
  $R''$   $NFSI$   $R''$   $N(SO_2Ph)_2$ 

complex	yield (%) <sup>a</sup>
1+	$21 \pm 1^{b}$
$2^{\scriptscriptstyle{+}}$	$56 \pm 1 \ (75)^c$
$3^{\scriptscriptstyle +}$	$58 \pm 4 (78)^c$
<b>4</b> <sup>+</sup>	$48 \pm 2 (70)^c$

<sup>a</sup>Reaction conditions: 2 equiv NFSI, CD<sub>3</sub>CN, 25 °C, 15 min. Yields (%) were determined by  $^1$ H NMR vs 1,3,5-trimethoxybenzene as internal standard.  $^b$ The amination product was formed over 24 h.  $^c$ The yields in parentheses were obtained at -35 °C.

lacks the oxidation strength to oxidize efficiently  $\mathbf{1}^+$ , which has a higher  $Pd^{II/III}$  redox potential.

Pd-catalyzed allylic  $\bar{C}-H$  amination with NFSI was reported by Zhang et al. They proposed the amination products were formed upon the reductive elimination of the  $Pd^{II}(\eta^3$ -allyl)- $N(SO_2Ph)_2$  intermediates via a  $Pd^{0/II}$  catalytic cycle. However, they also proposed that a  $Pd^{II/IV}$  catalytic cycle could be an alternate mechanism for the formation of amination products. While their system requires high temperatures for the amination reaction, in our case, allylic amination occurs rapidly at room temperature. To explore the possible amination mechanisms, we have analyzed the oxidation of  $2^+-4^+$  with NFSI by EPR at -35 °C. Interestingly, using 1 equiv NFSI, no EPR signals were detected, and no color

changes occurred upon the oxidation of  $2^+-4^+$ . After the addition of 1 more equiv NFSI, the EPR spectra for the oxidation of  $2^+-4^+$  reveal isotropic signals with the  $g_{ave}$  values of 2.080 (Figure S17a-c). In the EPR spectra for the oxidation of  $2^+-4^+$ , the superhyperfine coupling constant of  $A_z(2N) =$ 29.0 G in the  $g_z$  region is attributed to the interaction with the two axial N atoms (I = 1), suggesting that an octahedral geometry is maintained in solution. Surprisingly, this superhyperfine coupling constant of  $A_z(2N) = 29.0$  G is larger and comparable to the superhyperfine coupling constant of  $A_z(2N)$ = 24.0 G observed in  $\eta^3$ -2<sup>2+</sup> and 4<sup>2+</sup>. In addition, the EPR signals are stable even after a 30-min warmup at RT. These results led us to propose that the observed species are no longer containing allyl ligands bound to the  $Pd^{III}$  center, and a possible Pd-solvento species  $[(MeN4)Pd^{III}(MeCN)_2]^{3+}$  is formed in solution. To confirm this hypothesis, the [(MeN4)-Pd<sup>II</sup>(MeCN)<sub>2</sub>]<sup>2+</sup> complex was independently synthesized and oxidized with 1 equiv NFSI to generate the [(MeN4)- $Pd^{III}(MeCN)_2]^{3+}$  complex. The EPR spectrum of  $[(MeN4)-Pd^{III}(MeCN)_2]^{3+}$  displays an isotropic signal with the  $g_{ave}$  value of 2.063 (Figure S17d), which is similar to the EPR spectra obtained upon the oxidation of  $2^+-4^+$  with 2 equiv NFSI. The  $g_{\text{ave}}$  values of the EPR signals obtained upon the oxidation of 2<sup>+</sup>-4<sup>+</sup> with 2 equiv NFSI are only slightly larger than that observed for the [(MeN4)PdIII(MeCN)2]3+ complex, which could potentially be due to the N(SO<sub>2</sub>Ph)<sub>2</sub> anion or the F anion binding to the Pd<sup>III</sup> center. The superhyperfine coupling constant of  $A_z(2N) = 29.0$  G observed for [(MeN4)-Pd<sup>III</sup>(MeCN)<sub>2</sub>]<sup>3+</sup> is also consistent with the superhyperfine coupling constants  $A_z(2N) = 29.0$  G observed for the oxidation of of 2+-4+ with 2 equiv NFSI. Overall, these results strongly suggest that the oxidation of  $2^+-4^+$  with 2 equiv NFSI leads to the formation of the  $[(^{Me}N4)Pd^{III}(MeCN)_2]^{3+}$  complex, which likely forms upon the one-electron oxidation by NFSI of the in situ-generated  $[(MeN4)Pd^{II}(MeCN)_2]^{2+}$  species. Since NFSI can also act as a two-electron oxidant 56-58 and the high-valent  $Pd^{IV}(allyl)$  complexes prefer to adopt a  $\eta^1$ -allyl coordination mode, we propose that upon two-electron oxidation of  $2^+-4^+$ ,  $[(MeN4)Pd^{IV}(\eta^1-allyl)F]^{2+}$  species are generated as the key intermediates. The formation of only terminal amines during the oxidatively induced amination provides further evidence for  $\eta^1$ -allyl coordination in these (MeN4)Pd<sup>IV</sup> intermediates. Overall, we propose a mechanism of allylic amination in which the (MeN4)PdII complexes 2+-4+ undergo two-electron oxidation by NFSI to generate a (MeN4)Pd<sup>IV</sup>( $\eta^1$ -allyl) intermediate  $7^{2+}$ , followed by an S<sub>N</sub>2type reductive elimination involving the -N(SO<sub>2</sub>Ph)<sub>2</sub> anion to form the terminal allylic amines and  $8^{2+}$  (Scheme 4). Subsequent one-electron oxidation of 82+ by excess NFSI generates 9<sup>3+</sup>, which was confirmed experimentally.

#### CONCLUSIONS

In conclusion, herein, we report the synthesis and characterization of Pd(allyl) complexes supported by the tetradentate pyridinophane  $^{\rm R}{\rm N4}$  ligands. We observed that the nature of allyl moiety can affect the stability of the corresponding Pd^III complexes, with the  $[(^{\rm Me}{\rm N4}){\rm Pd}^{\rm III}(\eta^3\text{-}2\text{-methylallyl})]^{2+}$  complex being most stable. Furthermore, a rearrangement between the  $\eta^3\text{-allyl}$  and the  $\eta^1\text{-allyl}$  coordination modes was observed for the first time via EPR at a Pd^III center. Interestingly, a fast amination reaction occurred under mild conditions via high-valent Pd^IV( $\eta^1\text{-allyl})$  intermediates to generate terminal amines in high yields, especially at a lower temperature. Overall, these

Scheme 4. Proposed Mechanism for the Formation of Amination Products

stoichiometric reactivity and mechanistic studies set the stage for developing fast Pd-mediated allylic functionalization reactions involving high-valent Pd intermediates.

#### ASSOCIATED CONTENT

#### **5** Supporting Information

The Supporting Information is available free of charge at https://pubs.acs.org/doi/10.1021/acs.organomet.2c00215.

Synthetic details, spectroscopic characterization, stoichiometric and catalytic reactivity studies, and crystallographic data (PDF)

Cartesian coordinates of the computed optimized structures (TXT)

#### **Accession Codes**

CCDC 2006990–2006993 contain the supplementary crystallographic data for this paper. These data can be obtained free of charge via <a href="www.ccdc.cam.ac.uk/data\_request/cif">www.ccdc.cam.ac.uk/data\_request/cif</a>, or by emailing <a href="data\_request@ccdc.cam.ac.uk">data\_request/cif</a>, or by contacting The Cambridge Crystallographic Data Centre, 12 Union Road, Cambridge CB2 1EZ, UK; fax: +44 1223 336033.

#### AUTHOR INFORMATION

#### **Corresponding Author**

Liviu M. Mirica — Department of Chemistry, University of Illinois at Urbana-Champaign, Urbana, Illinois 61801, United States; orcid.org/0000-0003-0584-9508; Email: mirica@illinois.edu

#### **Authors**

Yung-Ching Wang — Department of Chemistry, University of Illinois at Urbana-Champaign, Urbana, Illinois 61801, United States

Nigam P. Rath — Department of Chemistry and Biochemistry, University of Missouri — St. Louis, St. Louis, Missouri 63121-4400, United States

Complete contact information is available at: https://pubs.acs.org/10.1021/acs.organomet.2c00215

#### **Notes**

The authors declare no competing financial interest.

#### ACKNOWLEDGMENTS

The authors thank the Department of Energy's BES Catalysis Science Program (DE-SC0006862) for financial support of the initial studies, and the authors also wish to thank the National Science Foundation (CHE-2102544) for financial support of the subsequent reactivity and EPR studies.

#### REFERENCES

- (1) Trost, B. M. Metal catalyzed allylic alkylation: its development in the Trost laboratories. *Tetrahedron* **2015**, *71*, 5708–5733.
- (2) Fernandes, R. A.; Nallasivam, J. L. Catalytic allylic functionalization via  $\pi$ -allyl palladium chemistry. *Org. Biomol. Chem.* **2019**, *17*, 8647–8672.
- (3) Tsuji, J.; Takahashi, H.; Morikawa, M. Organic Syntheses by Means of Noble Metal Compounds. 17. Reaction of  $\pi$ -Allylpalladium Chloride with Nucleophiles. *Tetrahedron Lett.* **1965**, 4387–4388.
- (4) Braun, M. G.; Doyle, A. G. Palladium-Catalyzed Allylic C-H Fluorination. J. Am. Chem. Soc. 2013, 135, 12990–12993.
- (5) Trost, B. M.; Crawley, M. L. Asymmetric transition-metal-catalyzed allylic alkylations: Applications in total synthesis. *Chem. Rev.* **2003**, *103*, 2921–2943.
- (6) Canty, A. J. Development of organopalladium(IV) chemistry: fundamental aspects and systems for studies of mechanism in organometallic chemistry and catalysis. *Acc. Chem. Res.* **1992**, 25, 83–90.
- (7) Lyons, T. W.; Sanford, M. S. Palladium-Catalyzed Ligand-Directed C-H Functionalization Reactions. *Chem. Rev.* **2010**, *110*, 1147–1169.
- (8) Muñiz, K. High-Oxidation-State Palladium Catalysis: New Reactivity for Organic Synthesis. *Angew. Chem., Int. Ed.* **2009**, 48, 9412–9423.
- (9) Canty, A. J. Organopalladium and platinum chemistry in oxidising milieu as models for organic synthesis involving the higher oxidation states of palladium. *Dalton Trans.* **2009**, 10409–10417.
- (10) Chen, X.; Engle, K. M.; Wang, D. H.; Yu, J. Q. Palladium(II)-Catalyzed C-H Activation/C-C Cross-Coupling Reactions: Versatility and Practicality. *Angew. Chem., Int. Ed.* **2009**, *48*, 5094–5115.
- (11) Sehnal, P.; Taylor, R. J. K.; Fairlamb, I. J. S. Emergence of Palladium(IV) Chemistry in Synthesis and Catalysis. *Chem. Rev.* **2010**, *110*, 824–889.
- (12) Desai, L. V.; Hull, K. L.; Sanford, M. S. Palladium-catalyzed oxygenation of unactivated sp(3) C-H bonds. *J. Am. Chem. Soc.* **2004**, 126, 9542–9543.
- (13) Xu, L.-M.; Li, B.-J.; Yang, Z.; Shi, Z.-J. Organopalladium(iv) chemistry. *Chem. Soc. Rev.* **2010**, *39*, 712–733.
- (14) Powers, D. C.; Ritter, T.Palladium(III) in Synthesis and Catalysis. In *Topics in Organometallic Chemistry*, Springer, 2011; Vol. 35, pp 129–156.
- (15) Khusnutdinova, J. R.; Rath, N. P.; Mirica, L. M. Stable Mononuclear Organometallic Pd(III) Complexes and Their C-C Bond Formation Reactivity. J. Am. Chem. Soc. 2010, 132, 7303–7305.
- (16) Pilarski, L. T.; Selander, N.; Bose, D.; Szabo, K. J. Catalytic Allylic C-H Acetoxylation and Benzoyloxylation via Suggested (eta(3)-Allyl)palladium(IV) Intermediates. *Org. Lett.* **2009**, *11*, 5518–5521.
- (17) Byers, P. K.; Canty, A. J. Organopalladium(IV) Chemistry Oxidative Addition of Organohalides to Dimethylpalladium(II) Complexes to Form Ethyl, Sigma-Benzyl, and Sigma-Allylpalladium-(IV) Complexes. *Chem. Commun.* **1988**, 639–641.
- (18) Guo, R. Y.; Portscheller, J. L.; Day, V. W.; Malinakova, H. C. An allylpalladium(IV) intermediate in the synthesis of highly

- substituted benzoxepines and benzopyrans via reactions of stable Pallada(II)cycles with allyl bromides. *Organometallics* **200**7, *26*, 3874—3883.
- (19) Xu, L. M.; Li, B. J.; Yang, Z.; Shi, Z. J. Organopalladium(IV) chemistry. *Chem. Soc. Rev.* **2010**, 39, 712–733.
- (20) Khusnutdinova, J. R.; Rath, N. P.; Mirica, L. M. The Aerobic Oxidation of a Pd(II) Dimethyl Complex Leads to Selective Ethane Elimination from a Pd(III) Intermediate. *J. Am. Chem. Soc.* **2012**, *134*, 2414–2422.
- (21) Tang, F.; Zhang, Y.; Rath, N. P.; Mirica, L. M. Detection of Pd(III) and Pd(IV) Intermediates during the Aerobic Oxidative C-C Bond Formation from a Pd(II) Dimethyl Complex. *Organometallics* **2012**, *31*, 6690–6696.
- (22) Tang, F. Z.; Qu, F. R.; Khusnutdinova, J. R.; Rath, N. P.; Mirica, L. M. Structural and reactivity comparison of analogous organometallic Pd(III) and Pd(IV) complexes. *Dalton Trans.* **2012**, *41*, 14046–14050.
- (23) Schultz, J. W.; Rath, N. P.; Mirica, L. M. Improved Oxidative C–C Bond Formation Reactivity of High-Valent Pd Complexes Supported by a Pseudo-Tridentate Ligand. *Inorg. Chem.* **2020**, *59*, 11782–11792.
- (24) Demunno, G.; Bruno, G.; Rotondo, E.; Giordano, G.; Loschiavo, S.; Piraino, P.; Tresoldi, G. Crystal-Structure of  $[Pd(\eta^3-2-Propenyl)(Dps)][Pd(\eta^3-2-Propenyl)Cl2]$  NMR Evidence of Binuclear  $\eta^3$ -Allyl Palladium(II) Species with Bridging Dps. *Inorg. Chim. Acta* 1993, 208, 67–75.
- (25) Hegedus, L. S.; Akermark, B.; Olsen, D. J.; Anderson, O. P.; Zetterberg, K. ( $\pi$ -Allyl)Palladium Complex Ion-Pairs Containing 2 Different, Mobile  $\pi$ -Allyl Groups NMR and X-Ray Crystallographic Studies. *J. Am. Chem. Soc.* **1982**, *104*, 697–704.
- (26) Mirica, L. M.; Khusnutdinova, J. R. Structure and electronic properties of Pd(III) complexes. *Coord. Chem. Rev.* **2013**, 257, 299–314.
- (27) Fuchigami, K.; Rath, N. P.; Mirica, L. M. Mononuclear Rhodium(II) and Iridium(II) Complexes Supported by Tetradentate Pyridinophane Ligands. *Inorg. Chem.* **2017**, *56*, 9404–9408.
- (28) Murrall, N. W.; Welch, A. J. Asymmetrically Bonded  $\pi$ -Ligands. 1. Hinging Away from Metal of Substituted Allyls Syntheses of 1-Syn-Methyl and 1-Syn-Phenyl Complexes, and the Molecular-Structures of  $[(\eta^1\text{-Ph-C3h4})\text{Pd}(\text{Tmeda})]\text{Bf4}, [(\eta\text{-C5h5})\text{Pd}(\eta^1\text{-Ph-C3h4})], and "[(Phen)Mo(Co)2(Ncs)(\eta^1\text{-Ph-C3h4})]. J. Organomet. Chem. 1986, 301, 109–130.$
- (29) Toniolo, L.; Boschi, T.; Deganello, G. Synthesis, characterization and fluxional behaviour of allylic palladium(II) carboxylate and N,N'- diarylformamidido complexes. *J. Organomet. Chem.* **1975**, 93, 405–414.
- (30) Lindley, J. Allyl palladium complexes: A simple experiment illustrating fluxional behavior. *J. Chem. Educ.* **1980**, *57*, *67*1.
- (31) Khusnutdinova, J. R.; Rath, N. P.; Mirica, L. M. The Conformational Flexibility of the Tetradentate Ligand <sup>tBu</sup>N4 is Essential for the Stabilization of (<sup>tBu</sup>N4)Pd<sup>III</sup> Complexes. *Inorg. Chem.* **2014**, *53*, 13112–13129.
- (32) Fulmer, G. R.; Miller, A. J. M.; Sherden, N. H.; Gottlieb, H. E.; Nudelman, A.; Stoltz, B. M.; Bercaw, J. E.; Goldberg, K. I. NMR Chemical Shifts of Trace Impurities: Common Laboratory Solvents, Organics, and Gases in Deuterated Solvents Relevant to the Organometallic Chemist. *Organometallics* **2010**, *29*, 2176–2179.
- (33) Kim, B. S.; Hussain, M. M.; Hussain, N.; Walsh, P. J. Palladium-Catalyzed Chemoselective Allylic Substitution, Suzuki-Miyaura Cross-Coupling, and Allene Formation of Bifunctional 2-B(pin)-Substituted Allylic Acetate Derivatives. *Chem. Eur. J.* **2014**, *20*, 11726–11739.
- (34) Fernandes, R. A.; Nallasivam, J. L. Catalytic allylic functionalization via pi-allyl palladium chemistry. *Org. Biomol. Chem.* **2019**, *17*, 8647–8672.
- (35) Pan, S. L.; Wu, B. Q.; Hu, J. J.; Xu, R. G.; Jiang, M.; Zeng, X. F.; Zhong, G. F. Palladium-Catalyzed Allylic Substitution Reaction of Benzothiazolylacetamide with Allylic Alcohols in Water. *J. Org. Chem.* **2019**, *84*, 10111–10119.

ı

**Organometallics** Article pubs.acs.org/Organometallics

- (36) Gao, P. S.; Li, N.; Zhang, J. L.; Zhu, Z. L.; Gao, Z. W.; Sun, H. M.; Zhang, W. Q.; Xu, L. W. Highly Efficient Palladium-Catalyzed Allylic Alkylation of Cyanoacetamides with Controllable and Chemoselective Mono- and Double Substitutions. ChemCatChem 2016, 8, 3466-3474.
- (37) Wang, J. H.; Dai, Z. H.; Xiong, C.; Zhu, J.; Lu, J. R.; Zhou, Q. F. Palladium-Catalyzed Allylic Alkylation of Aldimine Esters with Vinyl-Cyclopropanes to Yield alpha, alpha-Disubstituted alpha-Amino Acid Derivatives. Adv. Synth. Catal. 2019, 361, 5105-5111.
- (38) Hirata, G.; Satomura, H.; Kumagae, H.; Shimizu, A.; Onodera, G.; Kimura, M. Direct Allylic Amination of Allylic Alcohol Catalyzed by Palladium Complex Bearing Phosphine Borane Ligand. Org. Lett. 2017, 19, 6148-6151.
- (39) Feuerstein, M.; Laurenti, D.; Doucet, H.; Santelli, M. Efficiency of a tetraphosphine ligand in palladium catalysed allylic amination. J. Mol. Catal. A 2002, 182-183, 471-480.
- (40) Hickman, A. J.; Sanford, M. S. High-valent organometallic copper and palladium in catalysis. Nature 2012, 484, 177-185.
- (41) Dick, A. R.; Hull, K. L.; Sanford, M. S. A highly selective catalytic method for the oxidative functionalization of C-H bonds. J. Am. Chem. Soc. 2004, 126, 2300-2301.
- (42) Deprez, N. R.; Sanford, M. S. Synthetic and Mechanistic Studies of Pd-Catalyzed C-H Arylation with Diaryliodonium Salts: Evidence for a Bimetallic High Oxidation State Pd Intermediate. J. Am. Chem. Soc. 2009, 131, 11234-11241.
- (43) Powers, D. C.; Ritter, T. Bimetallic Pd(III) complexes in palladium-catalysed carbon-heteroatom bond formation. Nat. Chem. 2009, 1, 302-309.
- (44) Nielsen, M. C.; Lyngvi, E.; Schoenebeck, F. Chemoselectivity in the Reductive Elimination from High Oxidation State Palladium Complexes - Scrambling Mechanism Uncovered. J. Am. Chem. Soc. 2013, 135, 1978-1985.
- (45) Powers, D. C.; Benitez, D.; Tkatchouk, E.; Goddard, W. A.; Ritter, T. Bimetallic Reductive Elimination from Dinuclear Pd(III) Complexes. J. Am. Chem. Soc. 2010, 132, 14092-14103.
- (46) Cho, E. J.; Senecal, T. D.; Kinzel, T.; Zhang, Y.; Watson, D. A.; Buchwald, S. L. The Palladium-Catalyzed Trifluoromethylation of Aryl Chlorides. Science 2010, 328, 1679-1681.
- (47) Zhu, Q. H.; Ji, D. Z.; Liang, T. T.; Wang, X. Y.; Xu, Y. G. Efficient Palladium-Catalyzed C-H Fluorination of C(sp3)-H Bonds: Synthesis of beta-Fluorinated Carboxylic Acids. Org. Lett. 2015, 17, 3798-3801.
- (48) Yin, G. Y.; Mu, X.; Liu, G. S. Palladium(II)-Catalyzed Oxidative Difunctionalization of Alkenes: Bond Forming at a High-Valent Palladium Center. Acc. Chem. Res. 2016, 49, 2413-2423.
- (49) Testa, C.; Roger, J.; Fleurat-Lessard, P.; Hierso, J. C. Palladium-Catalyzed Electrophilic C-H-Bond Fluorination: Mechanistic Overview and Supporting Evidence. Eur. J. Org. Chem. 2019, 2019, 233-
- (50) Xiong, T.; Li, Y.; Mao, L. J.; Zhang, Q.; Zhang, Q. Palladiumcatalyzed allylic C-H amination of alkenes with N-fluorodibenzenesulfonimide: water plays an important role. Chem. Commun. 2012, 48, 2246-2248.
- (51) Haines, B. E.; Kawakami, T.; Kuwata, K.; Murakami, K.; Itami, K.; Musaev, D. G. Cu-Catalyzed aromatic C-H imidation with Nfluorobenzenesulfonimide: mechanistic details and predictive models. Chem. Sci. 2017, 8, 988-1001.
- (52) Halperin, S. D.; Fan, H.; Chang, S.; Martin, R. E.; Britton, R. A Convenient Photocatalytic Fluorination of Unactivated C-H Bonds. Angew. Chem., Int. Ed. 2014, 53, 4690-4693.
- (53) Halperin, S. D.; Kwon, D.; Holmes, M.; Regalado, E. L.; Campeau, L. C.; DiRocco, D. A.; Britton, R. Development of a Direct Photocatalytic C-H Fluorination for the Preparative Synthesis of Odanacatib. Org. Lett. 2015, 17, 5200-5203.
- (54) Rueda-Becerril, M.; Sazepin, C. C.; Leung, J. C. T.; Okbinoglu, T.; Kennepohl, P.; Paquin, J. F.; Sammis, G. M. Fluorine Transfer to Alkyl Radicals. J. Am. Chem. Soc. 2012, 134, 4026-4029.
- (55) Nodwell, M. B.; Bagai, A.; Halperin, S. D.; Martin, R. E.; Knust, H.; Britton, R. Direct photocatalytic fluorination of benzylic C-H

- bonds with N-fluorobenzenesulfonimide. Chem. Commun. 2015, 51, 11783-11786.
- (56) Lal, G. S.; Pez, G. P.; Syvret, R. G. Electrophilic NF fluorinating agents. Chem. Rev. 1996, 96, 1737-1755.
- (57) Antelo, J. M.; Crugeiras, J.; Leis, J. R.; Rios, A. Nucleophilic reactivity towards electrophilic fluorinating agents: reaction with Nfluorobenzenesulfonimide ((PhSO2)(2)NF). J. Chem. Soc., Perkin Trans. 2 2000, 2071-2076.
- (58) Rostami, A. N-fluorobenzenesulfonimide [(PhSO2)(2)NF] A neutral N-F-containing electrophilic fluorinating agent. Synlett 2007, 2007, 2924-2925.

### **□** Recommended by ACS

Effect of Precatalyst Oxidation State in C-N Cross-Couplings with 2-Phosphinoimidazole-Derived Bimetallic Pd(I) and Pd(II) Complexes

Erin E. Martinez, David J. Michaelis, et al.

AUGUST 03, 2021 ORGANOMETALLICS

Reactivity of a Dinuclear Pd<sup>I</sup> Complex [Pd<sub>2</sub>(μ-PPh<sub>2</sub>)(μ<sub>2</sub>-OAc)(PPh<sub>3</sub>)<sub>2</sub>] with PPh<sub>3</sub>: Implications for Cross-Coupling Catalysis Using the Ubiquitous Pd(OAc)<sub>2</sub>/...

Neil W. J. Scott, Ian J. S. Fairlamb, et al.

AUGUST 19, 2021 ORGANOMETALLICS

READ **C** 

**Computational Study of Intramolecular Coordination** Enhanced Oxidative Addition to form PdIV-Pincer Complexes, and Selectivity in Aryloxide Attack at P...

Allan J. Canty and Alireza Ariafard

APRIL 28, 2021 ORGANOMETALLICS

READ **C** 

Sequential Insertion of Alkynes, Alkenes, and CO into the Pd-C Bond of ortho-Palladated Primary Phenethylamines: from  $\eta^3$ -Allyl Complexes and Enla...

José-Antonio García-López, Isabel Saura-Llamas, et al.

JANUARY 29, 2021

ORGANOMETALLICS

READ 2

Get More Suggestions >